# Physics and Technology

## Emitters

### Materials

Infrared emitting diodes (IREDs) can be produced from a range of different III-V compounds. Unlike the elemental semiconductor silicon, the compound III-V semiconductors consists of two different elements of group three (e.g., Al, Ga, In) and five (e.g., P, As) of the periodic table. The bandgap energies of these compounds vary between 0.18 eV and 3.4 eV. However, the IREDs considered here emit in the near infrared spectral range between 800 nm and 1000 nm, and, therefore, the selection of materials is limited to GaAs and the mixed crystal $Ga_{1-X}Al_XAs$, $0 \leq X < 0.8$, made from the pure compounds GaAs and AlAs.

Infrared radiation is produced by radiative recombination of electrons and holes from the conduction and valence bands. The emitted photon energy, therefore, corresponds closely to the bandgap energy $E_g$. The emission wavelength can be calculated according to the formula $\lambda(\mu m) = 1.240 / E_g(eV)$. The internal efficiency depends on the band structure, the doping material and the doping level. Direct bandgap materials offer high efficiencies, because no photons are needed for recombination of electrons and holes. GaAs is a direct gap material and $Ga_{1-X}Al_XAs$ is direct up to X = 0.44. The doping species Si provides the best efficiencies and shifts the emission wavelength below the bandgap energy into the infrared spectral range by about 50 nm typically.

Charge carriers are injected into the material via pn junctions. Junctions of high injection efficiency are readily formed in GaAs and $Ga_{1-X}Al_XAs$. P-type conductivity can be obtained with metals of valency two, such as Zn and Mg, n-type conductivity with elements of valency six, such as S, Se and Te. However, silicon of valency four can occupy sites of III-valence and V-valence atoms, and, therefore, acts as donor and as acceptor. The conductivity type depends primarily on the material growth temperature. By employing exact temperature control, pn junctions can be grown with the same doping species Si on both sides of the junction. Ge, on the other hand, also has a valency of four, but occupies group V sites at high temperatures i.e., p-type.

Only monocrystalline material is used for IRED production. In the mixed crystal system $Ga_{1-X}Al_XAs$, $0 \leq X < 0.8$, the lattice constant varies only by about $1.5 \times 10^{-3}$. Therefore, monocrystalline layered structures of different $Ga_{1-X}Al_XAs$ compositions can be produced with extremely high structural quality. These structures are useful because the bandgap can be shifted from 1.40 eV (GaAs) to values beyond 2.1 eV which enables transparent windows and heterogeneous structures to be fabricated. Transparent windows are another suitable means to increase efficiency, and heterogeneous structures can provide shorter switching times and higher efficiency. Such structures are termed double heterostructures (DH) and consist normally of two layers that confine a layer with a much smaller bandgap.

The best production method for all materials needed is liquid phase epitaxy (LPE). This method uses Ga-solutions containing As, possibly Al, and the doping substance. The solution is saturated at high temperature, typically 900°C, and GaAs substrates are dipped into the liquid. The solubility of As and Al decreases with decreasing temperature. In this way epitaxial layers can be grown by slow cooling of the solution. Several layers differing in composition may be obtained using different solutions one after another, as needed e.g. for DHs.

In liquid phase epitaxial reactors, production quantities of up to 50 wafers, depending on the type of structure required, can be handled .

### IRED Chips and Characteristics

At present, the most popular IRED chip is made only from GaAs. The structure of the chip is displayed in figure 5.

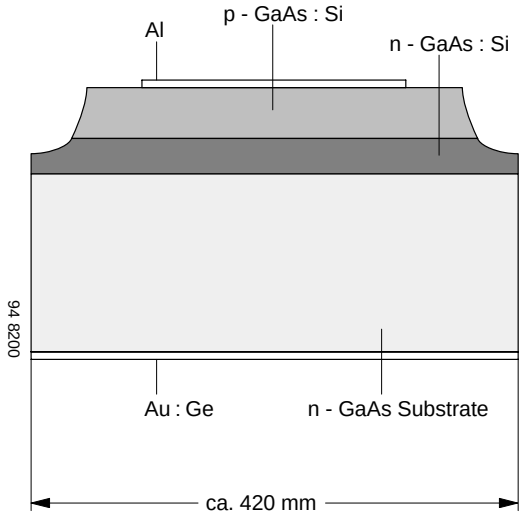


Figure 5.

On an n-type substrate, two Si-doped layers are grown by liquid phase epitaxy from the same solution. Growth starts as n-type at high temperature and becomes p-type below about 820°C. A structured Al-contact on the p-side and a large area Au:Ge contact on the back side provide a very low series resistance.

The angular distribution of the emitted radiation is displayed in figure 6.

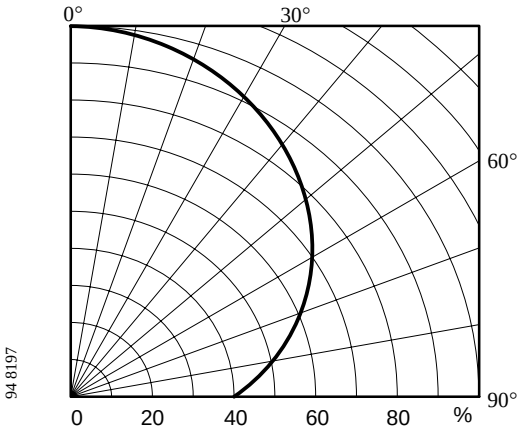


Figure 6.

The package of the chip has to provide good collection efficiency of the radiation emitted sideways, and has to diminish the refractive index step between the chip (n = 3.6) and the air (n = 1.0) with an epoxy of refractive index 1.55. In this way, the output power of the chip is increased by a factor of 3.5 for the assembled device.

The chip described is the most cost-efficient chip. The forward voltage at $I_F$ = 1.5 A has the lowest possible value. The total series resistance is typically only 0.60 Ω. The output power and the linearity (defined as the optical output power increase, divided by the current increase between 0.1 and 1.5 A) are high. Relevant data on the chip and a typical assembled device are given in table 2.

The technology used for another chip eliminates the absorbing substrate and uses only a thick epitaxial layer. The chip is shown in figure 7.

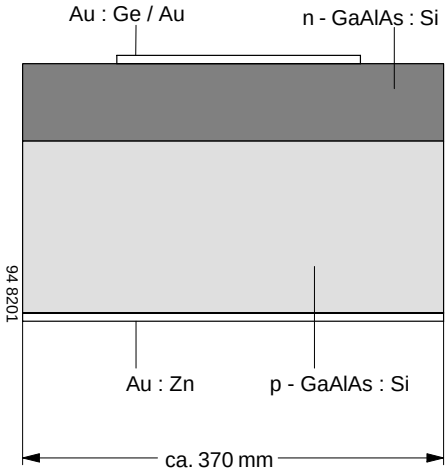


Figure 7.

Originally, the GaAs substrate was adjacent to the n-side. Growth of $Ga_{0.7}Al_{0.3}As$ started as n-type and became p-type – as in the first case – through the specific properties of the doping material Si. A characteristic feature of the Ga-Al-As phase system causes the Al-content of the growing epitaxial layer to decrease. This causes the Al-concentration at the junction to drop to 8% ($Ga_{0.92}Al_{0.08}As$), producing an emission wavelength of 880 nm. During further growth the Al-content approaches zero. The gradient of the Al-content and the correlated gradient of the bandgap energy, produces an emission band of a relatively large half width. The transparency of the large bandgap material results in a very high external efficiency on this type of chip.

The chip is mounted n-side up, and the front side metallization is Au:Ge/Au, whereas the reverse side metallization is Au:Zn.

The angular distribution of the emitted radiation is displayed in figure 8.

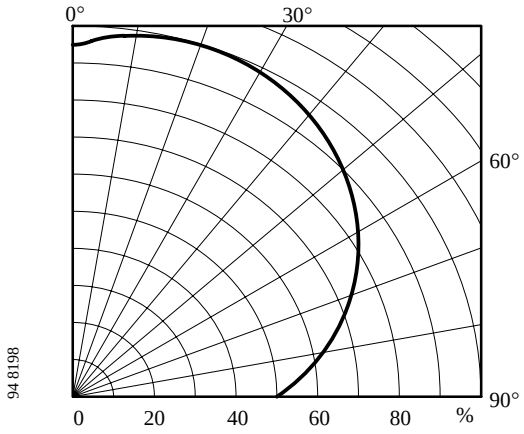


Figure 8.

The $Ga_{1-X}Al_XAs$ chip described has one of the highest output powers of any chip available. Due to its shorter wavelength, the chip offers specific advantages in combination with a Si detector. Integrated Opto-ICs, like amplifiers or Schmitt Triggers, have higher sensitivities at shorter wavelengths. Similarly, phototransistors are also more sensitive. Finally, the frequency bandwidth of pin diodes is higher at shorter wavelengths. This chip also has the advantage of having high linearity up to and beyond 1.5 A. The forward voltage, however, is higher than the voltage of a GaAs chip. Table 2 provides more data on the chip.

A technology combining some of the advantages of the two technologies described above is summarized in figure 9.

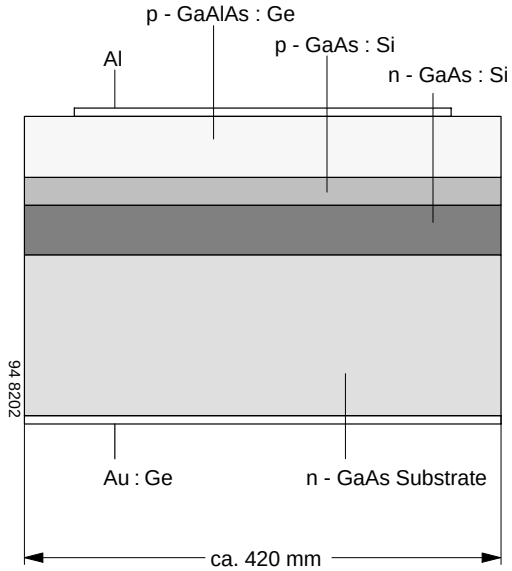


Figure 9.

Starting with the n-type substrate, n- and p-type GaAs layers are grown in a similar way to the epitaxy of the standard GaAs:Si diode. After this, a highly transparent window layer of $Ga_{1-X}Al_XAs$, doped p-type with Ge, is grown. The upper contact to the p-side is made of Al and the rear side contact is Au:Ge. The angular distribution of the emitted radiation is shown in figure 10.

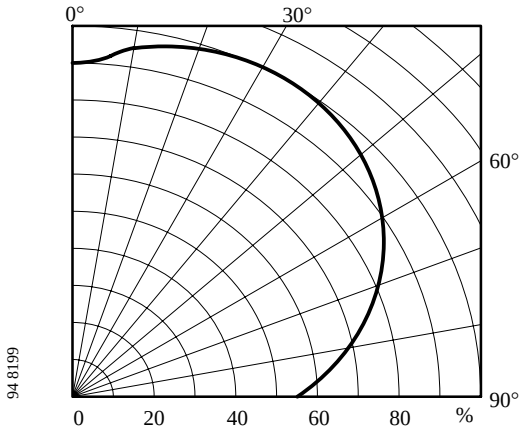


Figure 10.

This chip type combines a relatively low forward voltage with a high electro-optical efficiency, offering optimized combination between the advantageous characteristics of the two other chips. Refer again to table 2 for more details.

As mentioned in the previous section, double heterostructures (DH) provide even higher efficiencies and faster switching times. A schematical representation of such a chip is shown in figure 11.

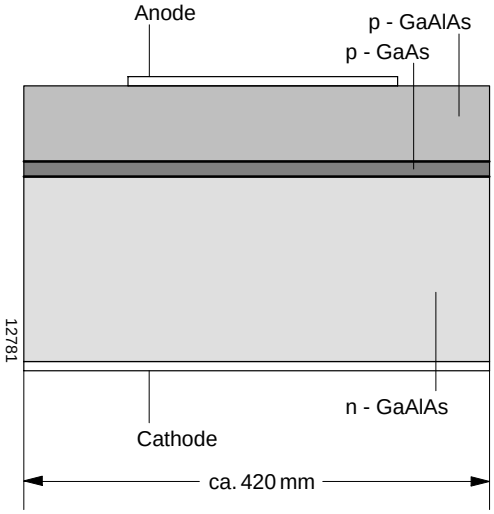


Figure 11.

The active layer is depicted as the thin layer between the p- and n-type $Ga_{1-X}Al_XAs$ confinement layers. The contacts are dependent on the polarity of the chip. If p is up, then the p-side contact is Al, the back side Au:Ge, and if n is up, then this side has a Au:Ge contact and the back side Au:Zn.Two such chips that are also very suitable for IrDA applications are given in table 2.

Table 2. Characteristic data of IRED chips

| Technology | Typical Chip Data | | | | Typical Device | Typical Device Data | | | | |
|---|---|---|---|---|---|---|---|---|---|---|
| | Φe/mW at 0.1 A | λp/nm | Δλ/nm | Polarity | | Φe/mW at 0.1 A | Φe/mW at 1.5 A | $V_F$/V at 0.1 A | $V_F$/V at 1.0 A | Φe(1.5A)/ Φe(0.1A) |
| GaAs on GaAs | 4.3 | 950 | 50 | p up | TSUS 540. | 15 | 140 | 1.3 | 2.1 | 9 |
| $Ga_{1-X}Al_XAs$ | 6.7 | 875 | 80 | n up | TSHA 550. | 27 | 350 | 1.5 | 3.4 | 13 |
| GaAs + $Ga_{1-X}Al_XAs$ on GaAs | 5.8 | 950 | 50 | p up | TSAL6200 | 35 | 300 | 1.35 | 2.4 | 12 |
| $Ga_{1-X}Al_XAs$ on $Ga_{1-X}Al_XAs$ | 11 | 870 | 40 | p up | TSHF 540. | 32 | | 1.3 | | $t_r$,$t_f$ /ns 30 |
| $Ga_{1-X}Al_XAs$ on $Ga_{1-X}Al_XAs$ | 16 | 870 | 40 | n up | TSPF 5400 | 40 | | 1.5 | | 30 |

## UV, Visible, and Near IR Silicon Photodetectors

(adapted from "Sensors, Vol 6, Optical Sensors, Chapt. 8, VCH – Verlag, Weinheim 1991)

### Silicon Photodiodes (PN and PIN Diodes)

**The physics of silicon detector diodes**

The absorption of radiation is caused by the interaction of photons and the charge carriers inside a material. The different energy levels allowed and the band structure determine the likelihood of interaction and, therefore, the absorption characteristics of the semiconductors. The long wavelength cutoff of the absorption is given by the bandgap energy. The slope of the absorption curve depends on the physics of the interaction and is much weaker for silicon than for most other semiconducting materials. This results in the strong wavelength-dependent penetration depth which is shown in figure 12. (The penetration depth is defined as that depth where 1/e of the incident radiation is absorbed.)

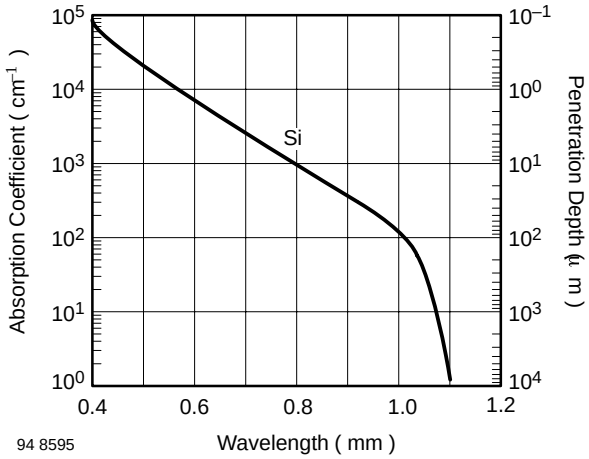


Figure 12. Absorption and penetration depth of optical radiation in silicon

Depending on the wavelength, the penetration depth varies from tenths of a micron at 400 nm (blue) to more than 100 μm at 1 μm (IR). For detectors to be effective, an interaction length of at least twice the penetration depth should be realized (equivalent to $1/e^2 = 86\%$ absorbed radiation). In the pn diode, the generated carriers are collected by the electrical field of the pn junction. The effects in the vicinity of a pn junction are shown in figure 13 for various types and operating modes of the pn diode. The incident radiation generates mobile minority carriers – electrons in the p-side, holes in the n-side. In the short circuit mode shown in figure 13 (top), the carriers drift under the field of the built-in potential of the pn junction.

Other carriers diffuse inside the field-free semiconductor along a concentration gradient, which results in an electrical current through the applied load, or without load, in an external voltage, the open circuit voltage, $V_{OC}$, at the contact terminals. The bending of the energy bands near the surface is caused by surface states. An equilibrium is established between the generation, the recombination of carriers, and the current flow through the load.

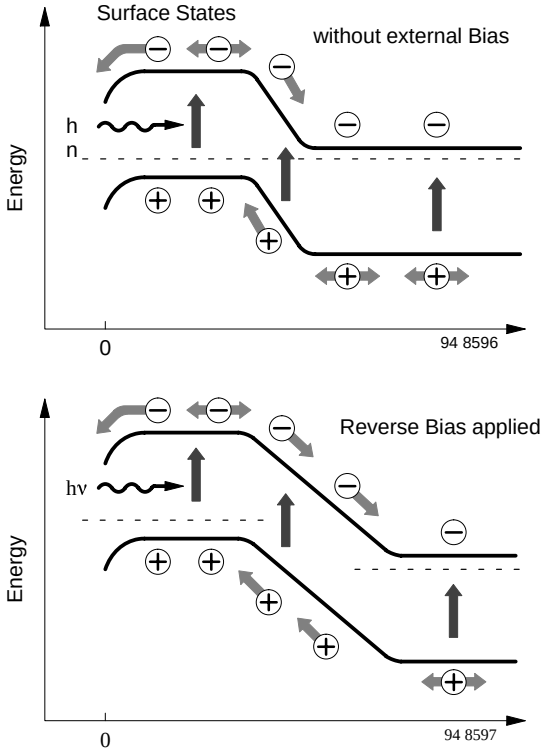


Figure 13. Generation-recombination effects in the vicinity of a pn junction. Top: Short circuit mode, bottom: reverse biased

The recombination takes place inside the bulk material with technology- and process-dependent time constants which are very small near the contacts and the surfaces of the device. For short wavelengths with very small penetration depths, the carrier recombination is the efficiency limiting process. To achieve high efficiencies, as many carriers as possible should be separated by the electrical field inside the space charge region. This is a very fast process, much faster than the typical recombination times (for data, see chapter 'Operating modes and circuits'). The width, W, of the space charge is a function of the doping concentration $N_B$ and the applied voltage V:

$$W = \sqrt{\frac{2 \times \epsilon_s \times (V_{bi} + V)}{q \times N_B}} \qquad (1.1)$$

(for a one-sided abrupt junction), where $V_{bi}$ is the built-in voltage, $\varepsilon_S$ the dielectric constant of Si, and q the electronic charge. The diode's capacitance (which can be speed limiting) is also a function of space charge width and applied voltage. It is given by

$$C = \frac{\epsilon_s \times A}{W}$$

where A is the area of the diode. An externally applied bias will increase the space charge width (see figure 13) with the result that a larger number of carriers are generated inside this zone which can be flushed out very fast with high efficiency under the applied field. From equation (1.1), it is evident that the space charge width is a function of the doping concentration $N_B$.

Diodes with a so-called pin structure show a wide space charge width where i stands for intrinsic, very low doped. This zone is also sometimes nominated as ν or p rather than low doped n, $n^-$ or p, $p^-$zone indicating the very low doping.

In figure 14, the different behavior of low doped pin diodes and pn diodes is shown. The space charge width of the pin diode (bottom) with a doping level ($n=N_B$) as low as $N_B = 5 \times 10^{11}$ $cm^{-3}$ is about 80 µm wide for a 2.5 V bias in comparison with a pn diode with a doping (n) of $N_B = 5 \times 10^{15}$ $cm^{-3}$ with only 0.8 µm.

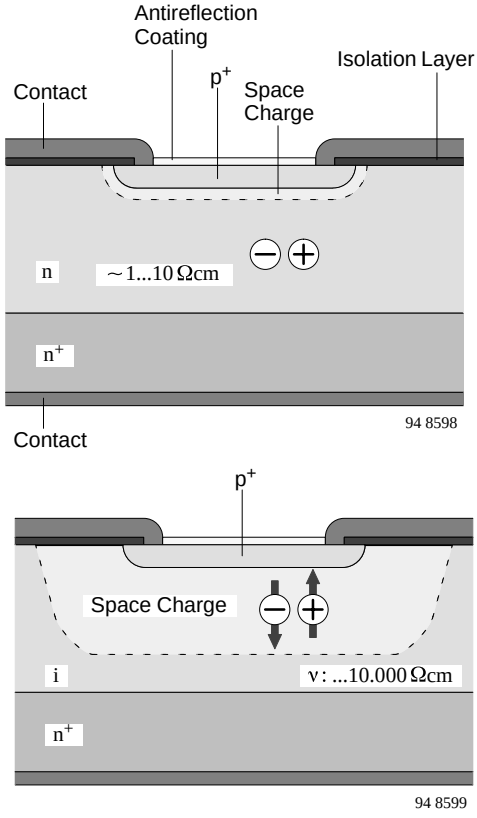


Figure 14. Comparison of pn diode (top) and pin diode (bottom)

## Properties of Silicon Photodiodes

### I-V Characteristics of illuminated pn junction

The cross section and the I-V-characteristics of a photodiode are shown in figure 15. The characteristic of the non illuminated diode is identical to the characteristic of a standard rectifier diode. The relationship between current, I, and voltage, V, is given by

$$I = I_S \times (\exp V/V_T - 1)$$

with $V_T = kT/q$
$k = 1.38 \times 10^{-23}$ JK$^{-1}$, Boltzmann constant
$q = 1.6 \times 10^{-19}$ As, electronic charge.

$I_S$, the dark-reverse saturation current, is a material and technology-dependent quantity. The value is influenced by the doping concentrations at the pn junction, by the carrier lifetime, and especially by the temperature. It shows a strongly exponential temperature dependence and doubles every 8°C.

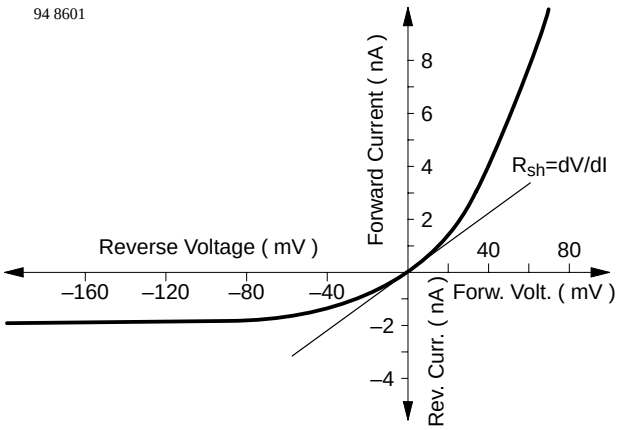


Figure 15. Measured I-V-characteristics of an Si photodiode in the vicinity of the origin

Typical dark currents of Si photodiodes are dependent on size and technology and range from less than picoamps up to tens of nanoamps at room temperature conditions. As noise generators, the dark current $I_{r0}$ and the shunt resistance $R_{sh}$ (defined and measured at a voltage of 10 mV forward or reverse, or peak-to-peak) are limiting quantities when detecting very small signals.

The photodiode exposed to optical radiation (see figure 16) generates a photocurrent $I_r$ exactly proportional to the incident radiant power $\Phi_e$.

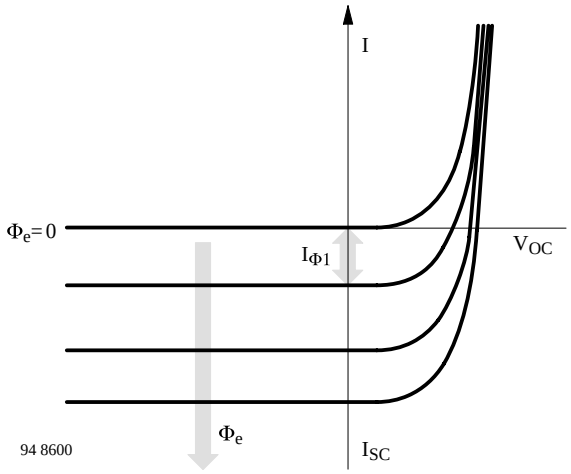


Figure 16. I-V-Characteristics of an Si photodiode under illumination. Parameter: Incident radiant flux

The quotient of both is the spectral responsivity s(λ),

$$s(\lambda) = I_r/\phi_e \ [A/W]$$

The characteristic of the irradiated photodiode is then given by

$$I = I_S \times (\exp V/V_T - 1) - s(\lambda) \times \phi_e$$

and in the case $V \approx 0$, zero or reverse bias we find,

$$I = -I_s - s(\lambda) \times \phi_e$$

Dependent on load resistance, $R_L$, and applied bias, different operating modes can be distinguished. The unbiased diode operates in the photovoltaic mode. Under short circuit conditions (load $R_L = 0\ \Omega$), the short circuit current, $I_{SC}$ flows into the load. When $R_L$ increases to infinity, the output voltage of the diode rises to the open circuit voltage, $V_{OC}$, given by

$$V_{OC} = V_T \times \ln( s(\lambda) \times \phi_e/I_s + 1)$$

Because of this logarithmic behavior, the open circuit voltage is sometimes used for optical lightmeters in photographic applications. The open circuit voltage shows a strong temperature dependence with a negative temperature coefficient. The reason for this is the exponential temperature coefficient of the dark reverse saturation current $I_S$. For precise light measurement, a temperature control of the photodiode is employed. Precise linear optical power measurements require small voltages at the load typically smaller than about 5% of the corresponding open circuit voltage. For less precise measurements, an output voltage of half the open circuit voltage can be allowed. The most important disadvantage of operating in the photovoltaic mode is the relative large response time. For faster response, it is necessary to implement an additional voltage source reverse biasing the photodiode. This mode of operation is termed the photoconductive mode.

In this mode, the lowest detectable power is limited by the shot noise of the dark current, $I_s$, while in the photovoltaic mode, the thermal (Johnson) noise of the shunt resistance, $R_{sh}$, is the limiting quantity.

**Spectral responsivity**

**Efficiency of Si photodiodes:**

The spectral responsivity, $s_\lambda$, is given as the number of generated charge carriers ($\eta \times N$) per incident photons N of energy $h \times \nu$ ($\eta$ is the percent efficiency, h is Plancks constant, and $\nu$ is the frequency of radiation). Each photon will generate one charge carrier at the most . The photocurrent $I_{re}$ is then given as

$$I_{re} = \eta \times N \times q$$

$$s_\lambda = I_{re}/\phi_e$$

$$= \eta \times N \times q/(h \times \nu \times N) = \eta \times q/(h \times \nu)$$

$$s_\lambda = \frac{\lambda(\mu m)}{1.24} \left[A/W\right]$$

At fixed efficiency, a linear relationship between wavelength and spectral responsivity is valid.

Figure 12 shows that semiconductors absorb radiation similar to a cut-off filter. At wavelengths smaller than the cut-off wavelength the incident radiation is absorbed. At larger wavelengths the radiation passes through the material without interaction. The cut-off wavelength corresponds to the bandgap of the material. As long as the energy of the photon is larger than the bandgap, carriers can be generated by absorption of photons, provided that the material is thick enough to propagate photon-carrier interaction. Bearing in mind that the energy of photons decreases with increasing wavelength, it can be understood, that the curve of the spectral responsivity vs. wavelength in the ideal case (100% efficiency) will have a triangular shape (see figure 17). For silicon photodetectors, the cut-off wavelength is near 1100 nm.

In most applications, it is not necessary to detect radiation with wavelengths larger than 1000 nm. Therefore, designers use a typical chip thickness of 200 µm to 300 µm, which results in reduced sensitivity at wavelengths larger than 950 nm . With a typical chip thickness of 250 µm, an efficiency of about 35% at 1060 nm is achieved. At shorter wavelengths (blue-near UV, 500 nm to 300 nm) the sensitivity is limited by recombination effects near the surface of the semiconductor. The reduction in the efficiency starts near 500 nm and increases with decreasing wavelength. Standard detectors designed for visible and near IR radiation may have only poor UV/blue sensitivity and poor UV stability. Well designed sensors for wavelengths of 300 to 400 nm can operate with fairly high efficiencies.
At smaller wavelengths (< 300 nm), the efficiency decreases strongly.

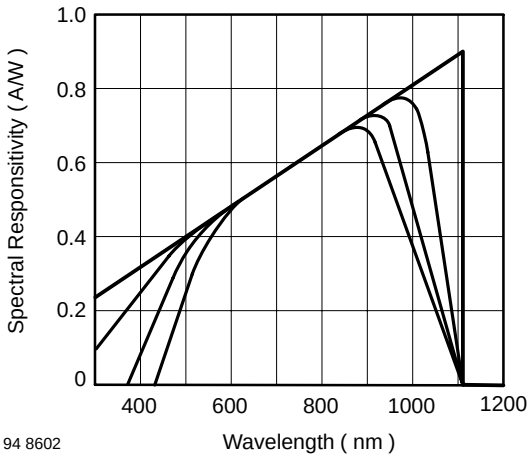


Figure 17. Spectral responsivity as a function of wavelength of a Si photodetector diode, ideal and typical values

**Temperature dependence of spectral responsivity**

The efficiency of carrier generation by absorption and the loss of carriers by recombination are the factors which influence the spectral responsivity. The absorption coefficient increases with temperature. Radiation of long wavelength is therefore more efficiently absorbed inside the bulk, and results in increased response. For shorter wavelengths (< 600 nm), reduced efficiency is observed with increasing temperature because of increased recombination rates near the surface. These effects are strongly dependent on technological parameters and therefore cannot be generalized to the behavior at longer wavelengths.

**Uniformity of spectral responsivity**

Inside the technologically defined active area of photodiodes, the spectral responsivity shows a variation of the sensitivity in the order of < 1%. Outside the defined active area, especially at the lateral edges of the chips, the local spectral response is sensitive to the applied reverse voltage. Additionally, this effect depends on the wavelength. Therefore, the relation between power (Watt) related spectral responsivity, $s_\lambda$ (A/W), and power density (Watt/cm$^2$) related spectral responsivity, $s_\lambda$ [A/(W/cm$^2$)] is not a constant. This relation is a function of wavelength and reverse bias.

### Stability of spectral responsivity

Si detectors for wavelengths between 500 nm and 800 nm appear to be stable over very long periods of time. In the literature concerned here, remarks can be found on instabilities of detectors in the blue, UV, and near IR under certain conditions.
Thermal cycling reversed the degradation effects.
Surface effects and contamination are possible causes but are technologically well controlled.

### Angular dependence of responsivity

The angular response of Si photodiodes is given by the optical laws of reflection. The angular response of a detector is shown in figure 18.

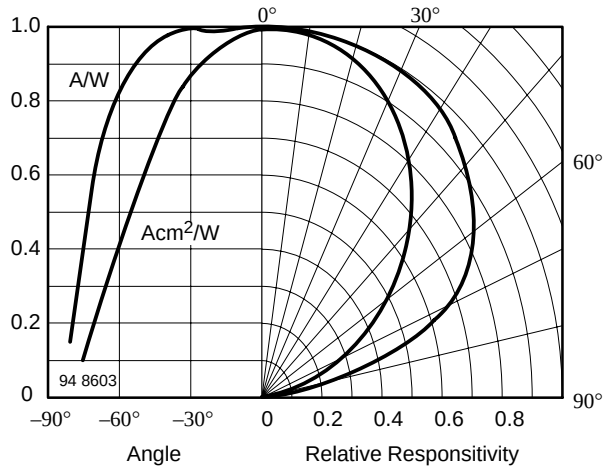


Figure 18. Responsivity of Si photodiodes as a function of the angle of incidence

The semiconductor surfaces are covered with quarter wavelength anti-reflection coatings. The encapsulation is performed with uncoated glass or sapphire windows.

The bare silicon response can be altered by optical imaging devices such as lenses. In this way, nearly every arbitrary angular response can be achieved.

### Dynamic Properties of Si Photodiodes

Si photodiodes are available in many different variations. The design of the diodes can be tailored to meet special needs. Si photodiodes may be designed for maximum efficiency at given wavelengths, for very low leakage currents, or for high speed. The design of a photodiode is nearly always a compromise between various aspects of a specification.

Inside the absorbing material of the diode, photons can be absorbed in different regions. For example at the top of a $p^+n^{--}$diode there is a highly doped layer of $p^+$-Si. Radiation of shorter wavelengths will be effectively absorbed, but for larger wavelengths only a small amount is absorbed. In the vicinity of the pn junction, there is the space charge region, where most of the photons should generate carriers. An electric field accelerates the generated carrier in this part of the detector to a high drift velocity. The carriers which are not absorbed in these regions penetrate into the field-free region where the motion of the generated carriers fluctuates by the slow diffusion process.

The dynamic response of the detector is composed of the different processes which transport the carriers to the contacts. The dynamic response of photodiodes is influenced by three fundamental effects:

- Drift of carriers in an electric field
- Diffusion of carriers
- Capacitance $\times$ load resistance

The carrier drift in the space charge region occurs rapidly with very small time constants. Typically, the transit times in an electric field of 0.6 V/µm are in the order of 16 ps/µm and 50 ps/µm for electrons and holes, respectively. At the (maximum) saturation velocity, transit time is in the order of 10 ps/µm for electrons in p-material. With a 10 µm drift region, travelling times of 100 ps can be expected. The response time is a function of the distribution of the generated carriers and is therefore dependent on the wavelength.
The diffusion of carriers is a very slow process. The time constants are in the order of some µs.
The typical pulse response of detectors is dominated by these two processes. Obviously, carriers should be absorbed in large space charge regions with high internal electrical fields. This requires material with an adequate low doping level. Furthermore, a reverse bias of rather large voltage is useful. Radiation of shorter wavelength is absorbed in smaller penetration depths. At wavelengths shorter than 600 nm, decreasing wavelength leads to an absorption in the diffused top layer. The movement of carriers in this region is also diffusion limited. Because of small carrier lifetimes, the time constants are not as large as in homogeneous substrate material.
Finally, the capacitive loading of the output in combination with the load resistance limits the frequency response.

### Properties of Silicon Phototransistors

The phototransistor is equivalent to a photodiode in conjunction with a bipolar transistor amplifier (figure 19). Typically, current amplification, B, is between 100 and 1000 depending on the type and application. The active area of the phototransistor is usually about $0.5 \times 0.5$ mm$^2$. Data of spectral responsivity are equivalent to those of photodiodes, but must be multiplied by the factor of the current amplification, B.

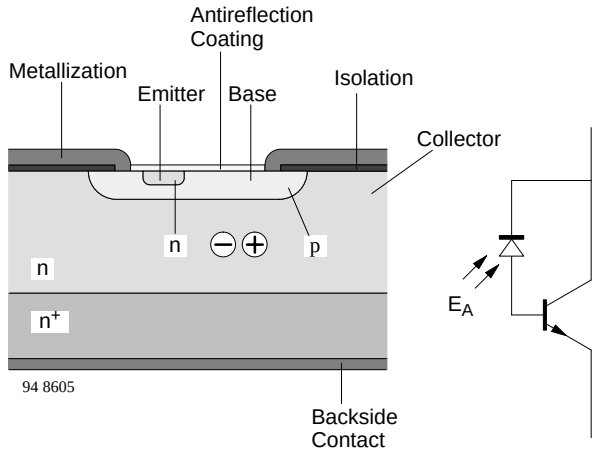


Figure 19. Phototransistor, cross section and equivalent circuit

The switching times of phototransistors are dependent on the current amplification and load resistance and are between 30 µs and 1 µs. The resulting cut-off frequencies are a few hundred kHz.

The transit times, $t_r$ and $t_f$, are given by

$$t_{r,f} = \sqrt{(1/2f_t^2)^2 + b(RC_BV)^2}$$

$f_t$: Transit frequency
R: Load resistance
$C_B$: Base-collector capacitance, b= 4...5
V: Amplification

Phototransistors are most frequently applied in interrupters and opto-isolators.

## Applications

Silicon photodetectors are used in manifold applications, such as sensors for radiation from the near UV over the visible to the near infrared. There are numerous applications in the measurement of light, such as dosimetry in the UV, photometry, and radiometry. A well known application is shutter control in cameras.

Another large application area for detector diodes and especially phototransistors, is that of position sensing. Examples are quadrant detectors, differential diodes, optical sensors, and reflex sensors.

Other types of silicon detectors are built-in as parts of optocouplers.

One of the largest application areas is the remote control of TV sets and other home entertainment appliances.

Different applications require specialized detectors and also special circuits to enable optimized functioning.

### Equivalent circuit

Photodetector diodes can be described by the electrical equivalent circuit shown in figure 20.

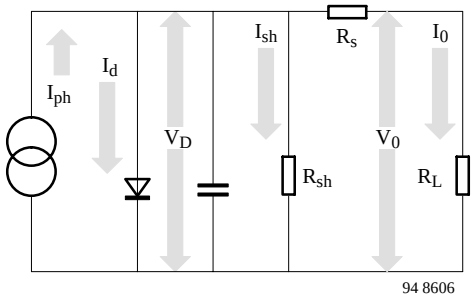


Figure 20.

$$I_O = I_{ph} - I_D - I_{sh}$$

$$I_O = I_{ph} - I_s\left(\exp\frac{qV_D}{kT} - 1\right) - I_{sh}$$

$$V_{OC} = V_T \times \ln\left(\frac{s(\lambda) \times \phi_e - I_{sh}}{I_s} + 1\right)$$

As described in chapter 'I-V Characteristics of illuminated pn junction', the incident radiation generates a photocurrent loaded by a diode characteristic and the load resistor, $R_L$. The other parts of the equivalent circuit (the parallel capacitance, C, combined from junction, $C_j$, and stray capacitances, the serial resistance, $R_S$, and the shunt resistance, $R_{sh}$, representing an additional leakage) can be neglected in most of the standard applications, and are not expressed in equations 2.3 and 2.4. However, in applications with high frequencies or extreme irradiation levels, these parts must be regarded as limiting elements.

### Searching for the right detector diode type

The photodiode BPW 20 R is a pn diode based on rather highly doped n-silicon, while the S153P is a pin diode based on very lightly doped n-silicon. Both diodes have the same active area and the spectral response as a function of the wavelength is very similar. The diodes differ in the junction capacitance and shunt resistance both of which can influence the performance in the application.

Detecting very small signals is the domain of the pn diodes with their very small dark currents and dark/shunt resistances.
With a specialized detector technology, these parameters are very well controlled in all Vishay photodetectors.

The very small leakage currents of pn diodes are offset by higher capacitances and smaller bandwidths in comparison to pin diodes.

Photodiodes are often operated in the photovoltaic mode (especially in light meters) , as depicted in the circuit of figure 21, where a strong logarithmic dependence of the open circuit voltage on the input signal is used.

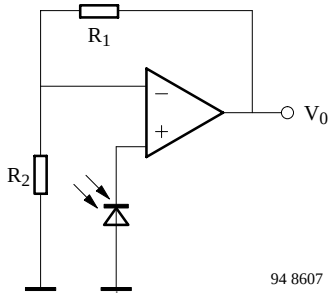


$$V_O \approx V_{OC} \times \left[1 + R_1/R_2\right] \quad \text{with}$$

$$V_{OC} = V_T \times \ln( s(\lambda) \times \phi_e/I_s + 1 )$$

Figure 21. Photodiode in the photovoltaic mode operating with a voltage amplifier

It should be noted that the extremely high shunt/dark resistance (more than 15 GΩ) combined with a high-impedance operational amplifier input and a junction capacitance of about 1 nF can result in slow switch-off time constants of some seconds. Some instruments therefore have a reset button for shortening the diode before starting a measurement. The photovoltaic mode of operation for precise measurements should be limited to the range of low ambient temperatures, or a temperature control of the diode (e.g., using a Peltier cooler) should be applied. At elevated temperatures, the dark current is increased (see figure 22) leading to a non-logarithmic and temperature dependent output characteristic (see figure 23). The curves shown in figure 22 represent the typical behavior of these diodes. The guaranteed leakage (dark reverse current) is specified with $I_{ro}$ = 30 nA for the standard types. This value is far from the one which is typically measured. Tighter customer specifications are available on request. The curves of figure 23 show the open circuit voltage as a function of the irradiance with the dark reverse current, $I_S$, as parameter (in a first approximation increasing $I_S$ and $I_{sh}$ have the same effect). The parameter covers the possible spread of dark current. In combination with figure 22 one can project the extreme dependence of the open circuit voltage at high temperatures (figure 24).

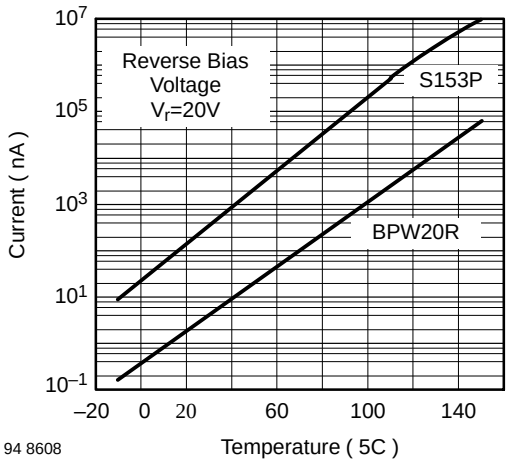


Figure 22. Dark reverse current vs. temperature

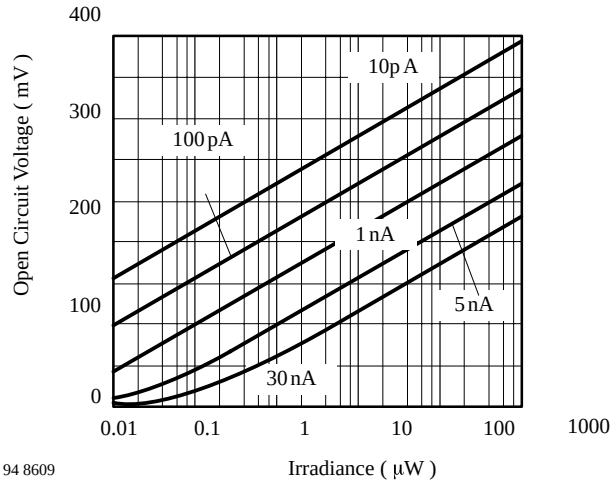


Figure 23. Open circuit voltage vs. irridiance, parameter: dark reverse current, BPW 20 R

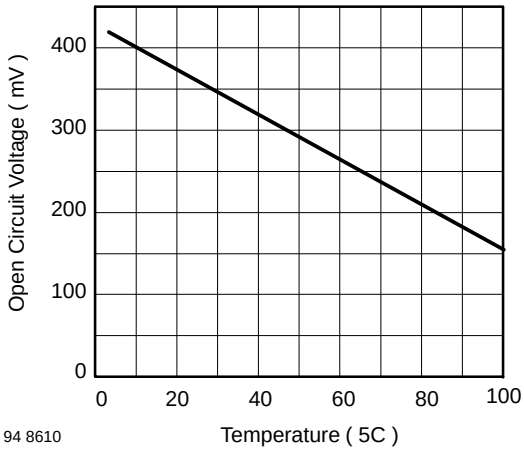


Figure 24. Open circuit voltage vs. temperature, BPW46

### Operating modes and circuits

The advantages and disadvantages of operating a photodiode in the open circuit mode have been discussed.

For operation in the short circuit (see figure 25) or photoconductive (see figure 26) mode, current-to-voltage converters are typically used. In comparison with the photovoltaic mode, the temperature dependence of the output signal is much lower. Generally the temperature coefficient of the light reverse current is positive for irradiation with wavelengths > 900 nm, rising with increasing wavelength. For wavelengths < 600 nm, a negative temperature coefficient is found, likewise with increasing absolute value to shorter wavelengths. Between these wavelength boundaries the output is almost independent of temperature. By using this mode of operation, reverse biased or unbiased (short circuit conditions), the output voltage, Vo, will be directly proportional to the incident radiation, $\phi_e$ (see the equation in figure 25).

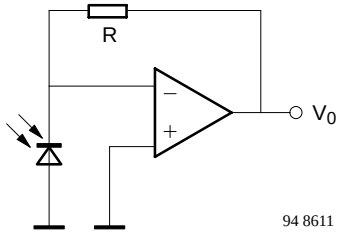


$$V_O = -R \times \Phi_e \times s(\lambda)$$

$$V_O = -I_{SC} \times R$$

Figure 25. Transimpedance amplifier, current to voltage converter, short circuit mode

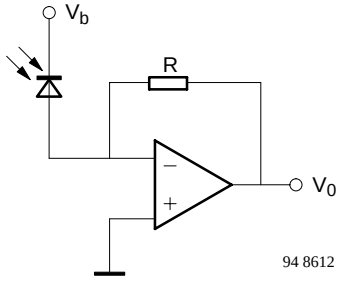


Figure 26. Transimpedance amplifier, current to voltage converter, reverse biased photodiode

The circuit in figure 25 minimizes the effect of the reverse dark current while the circuit in figure 26 improves the speed of the detector diode due to a wider space charge region with decreased junction capacitance and field increased velocity of the charge carrier transport.

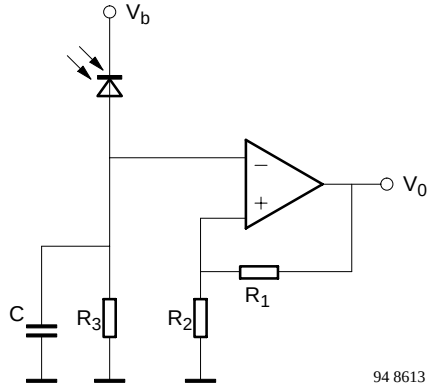


Figure 27. RC-loaded photodiode with voltage amplifier

Figure 27 shows photocurrent flowing into an RC load, where C represents the junction and stray capacitance while $R_3$ can be a real or complex load, such as a resonant circuit for the operating frequency.

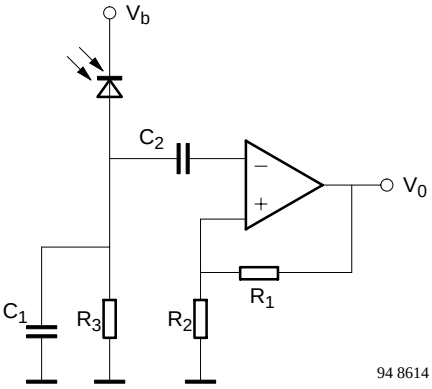


$$V_O \approx \phi_e \times s(\lambda) \times R_3 \times \left[1 + R_1/R_2\right]$$

Figure 28. AC-coupled amplifier circuit

The circuit in figure 28 is equivalent to figure 27 with a change to AC coupling. In this case, the influence of the background illumination can be separated from a modulated signal. The relation between input signal (irradiation, $\phi_e$) and output voltage is given by the equation in figure 28.

### Frequency response

The limitations of the switching times in pn diodes is determined by the carrier lifetime. Due to the absorption properties of silicon, especially in pn diodes, most of the incident radiation at longer wavelengths is absorbed outside the space charge region. Therefore, a strong wavelength dependence of the switching times can be observed (figure 29).

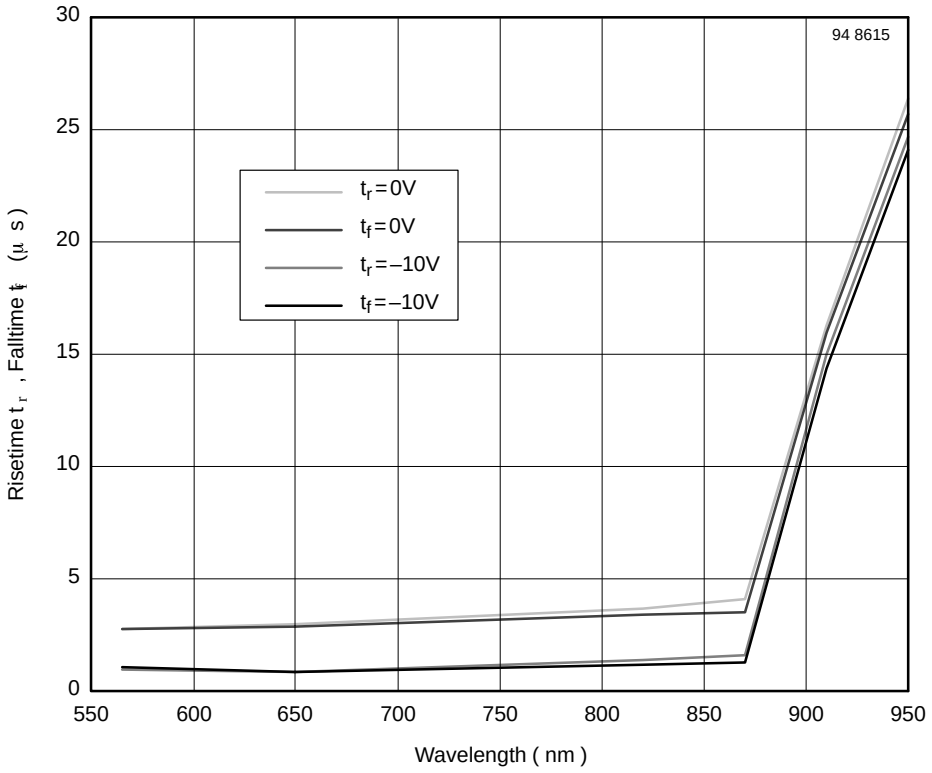


Figure 29. Switching times vs. wavelength for photodiode BPW 20 R

A drastic increase in rise and fall times is observed at wavelengths > 850 nm. The differences between unbiased and biased operation result from the widening of the space charge region.

However, for the pin diodes (BPW34/ S153P family) similar results with shifted time scales are found. This behavior, in this case in the frequency domain, is presented in figure 30 for a wavelength of 820 nm and figure 31. for 950 nm.

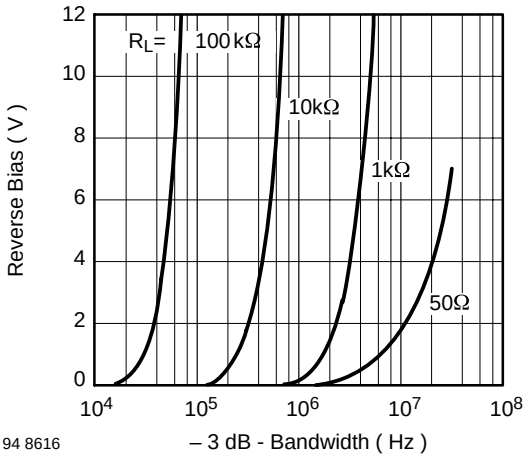


Figure 30. BPW 41-family, bandwidth vs. reverse bias voltage, parameter: load resistance, λ = 820 nm

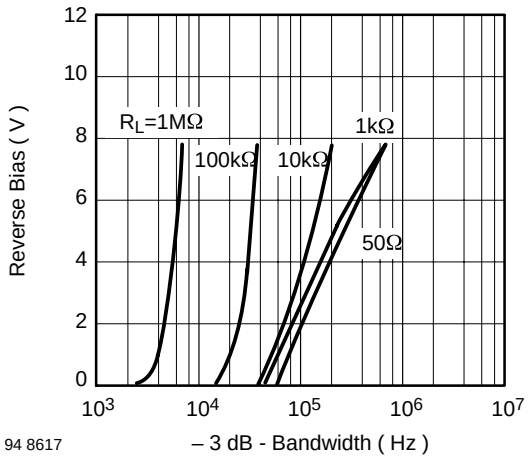


Figure 31. BPW 41-family, bandwidth vs. reverse bias voltage, parameter: load resistance, λ = 950 nm

Below about 870 nm, only slight wavelength dependence can be recognized, while a steep change of cut-off frequency takes place from 870 nm to 950 nm (different time scales in figure 30 and figure 31 !). Additionally, the influence of the load resistances and the reverse bias voltages can be taken from these diagrams.

For cut-off frequencies greater 10–20 MHz, depending on the supply voltage available for biasing the detector diode, pin diodes are also used. However, for this frequency range, and especially when operating with low bias voltages, thin epitaxially grown intrinsic (i) layers are incorporated into the pin diodes. As a result, these diodes (e.g., Vishays BPW97) can operate with low bias voltages (3 to 4 V) with cut-off frequencies of 300 MHz at a wavelength of 790 nm. With application-specific optimized designs, pin diodes with cutoff frequencies up to 1 GHz at only a 3 V bias voltage with only an insignificant loss of responsivity can be generated.

The main applications for these photodiodes are found in optical local area networks operating in the first optical window at wavelengths of 770 nm to 880 nm.

**Which type for which application?**

In table 3, selected diode types are assigned to different applications. For more precise selection according to chip sizes and packages, refer to the tables in the introductory pages of this data book.

Table 3. Photo diode reference table

| Detector application | pin diode | pn diode | epi-pin diode |
|---|---|---|---|
| Photometry, lightmeter | | BPW 21 R | |
| Radiometry | S 153 P, BPW 34, ... | BPW 20 R | |
| Light barriers | BPW 24 | | |
| Remote control<br>Low speed data transmission < 10 MHz, clear package | BPW 34, BPW 46, BPV 10 | | |
| IR filter for<br>λ > 900 nm included | BPV 20 F, BPV 23 F,<br>BPW 41 N, S 186 P,<br>TSOP-Series (with integrated amplifier and demodulator) | | |
| IR filter for<br>λ > 820 nm included | BPV 23 NF, BPW 82, BPW 83<br>BPV10NF | | |
| Fiber optical receiver | frequencies < 20 MHz<br>BPW 24 R | | high frequencies<br>BPW 97 |
| Densitometry | BPW 34, BPV 10, BPW 43 | BPW 20 R, BPW 21 R | |
| Smoke detector | BPV22NF | | |
| Data Transmission | BPV22NF | | |

## Phototransistor Circuits

A phototransistor typically is operated in a circuit as shown in figure 32. The resistor $R_B$ can be omitted in most applications. In some phototransistors, the base is not connected. $R_B$ can be used to suppress background radiation by setting a threshold level (see equation 5.1 and 5.2)

$$V_O = V_S - B \times \phi_e \times s(\lambda) \times R_L \quad (5.1)$$

$$V_O \approx V_S - (B \times \phi_e \times s(\lambda) - 0.6/R_B) \times R_L \quad (5.2)$$

For the dependence of the rise and fall times on the load resistance and collector-base capacitance refer to chapter 'Properties of Silicon Phototransistors'.

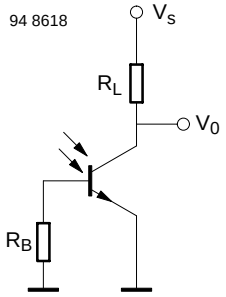


Figure 32. Phototransistor with load resistor and optional base resistor.